International Journal of Hydrogen Energy 130 (2025) 411–422

Contents lists available at ScienceDirect

International Journal of Hydrogen Energy

journal homepage: www.elsevier.com/locate/he

On-board hydrogen-rich syngas production via waste heat recovery from compression-ignition engines: maximizing hydrogen content with novel multi-objective algorithms

Ümit Ağbulut [a,b,c,*], Petr Vozka [a,**], Hüseyin Bakır [d], Nathan A. Brieu [a], Fikret Polat [e], Suat Sarıdemir [e]

[a] Department of Chemistry and Biochemistry, California State University, Los Angeles, State University Drive 5151, 90032, Los Angeles, CA, USA
[b] Department of Mechanical Engineering, Mechanical Engineering Faculty, Yildiz Technical University, Istanbul, 34349, Türkiye
[c] Department of Technical Sciences, Western Caspian University, Baku, Azerbaijan
[d] Department of Electronics and Automation, Vocational School, Dogus University, Istanbul, 34775, Türkiye
[e] Department of Mechanical Engineering, Faculty of Engineering, Düzce University, Düzce, 81620, Türkiye

ARTICLE INFO

Keywords:
Hydrogen-rich gas
Methanol-steam reforming
Waste heat recovery
Optimization algorithms

ABSTRACT

A significant portion of fuel energy in internal combustion engines is lost as waste heat, yet limited efforts have been made to recover it effectively. This research explores the utilization of exhaust heat from a diesel engine to produce H_2-rich syngas through the methanol-steam reforming (MSR) process. The engine operates at varying loads (15, 30, 45, and 60 Nm) while maintaining a constant speed of 2000 rpm. Exhaust heat is redirected to an MSR reactor, where the methanol-to-water (MtW) molar ratio is adjusted (0.5, 1, 1.5, and 2). Results reveal that the highest hydrogen content in syngas (70.3 %) is achieved at an engine load of 30 Nm and an MtW ratio of 1. To further optimize hydrogen production, three novel algorithms (DSC-MOPSO, MOSPO, and MOGWO) are applied to key operation parameters. Optimization increases hydrogen content to 72.5 % with DSC-MOPSO, 72.4 % with MOSPO, and 72.1 % with MOGWO, with error margins below 0.7 %.

Nomenclature

Abbreviations	
CI	Compression-Ignition
ICEs	Internal Combustion Engines
MSR	Methanol-Steam Reforming
MtW	Methanol-to-Water
EGT	Exhaust Gas Temperature
CFD	Computational Fluid Dynamics
IPCC	Intergovernmental Panel on Climate Change
ANOVA	Analysis of Variance
RT	Reaction Temperature
RP	Reactor Pressure
DSC	Dynamic Switched Crowding
PSO	Particle Swarm Optimization
GWO	Grey Wolf Optimizer
SPO	Stochastic Paint Optimizer
RSM	Response Surface Methodology
MOSPO	Multi-Objective Stochastic Paint Optimizer
MOGWO	Multi-Objective Grey Wolf Optimizer
DSC-MOPSO	Dynamic Switched Crowding-Based Multi-Objective Particle Swarm Optimization
Symbols	
Nm	Newton-Meter
rpm	Rotations Per Minute
H_2	Hydrogen
CO	Carbon Monoxide
CO_2	Carbon Dioxide
$CuGa_2O_4$	Copper Gallium Oxide
Cu/ZnO/Al_2O_3	Copper–Zinc Oxide-Aluminum Oxide
Al_2O_3	Aluminum Oxide
H_2O	Water
MeOH	Methanol
K	Kelvin

(continued on next column)

(continued)

(continued on next page)

* Corresponding author. Department of Chemistry and Biochemistry, California State University, Los Angeles, State University Drive 5151, 90032, Los Angeles, CA, USA.
** Corresponding author.
E-mail addresses: uagbulu@calstatela.edu (Ü. Ağbulut), pvozka@calstatela.edu (P. Vozka).

https://doi.org/10.1016/j.ijhydene.2025.04.261
Received 1 January 2025; Received in revised form 5 March 2025; Accepted 14 April 2025
Available online 27 April 2025
0360-3199/© 2025 The Authors. Published by Elsevier Ltd on behalf of Hydrogen Energy Publications LLC. This is an open access article under the CC BY-NC-ND license (http://creativecommons.org/licenses/by-nc-nd/4.0/).

(*continued*)

°C	Centigrade
Ni	Nickel
CH_4	Methane
atm	Atmospheric Pressure
kW	Kilowatt
cm^3	Cubic Centimeter
mm	Millimeter
Ni/Cr	Nickel–Chromium
B25	Waste Biodiesel Fuel of 25 % and Diesel fuel of %75 (v/v)
D100	Conventional Diesel Fuel
B25 + $15H_2$	B25 + 15 lpm hydrogen
B25 + $30H_2$	B25 + 30 lpm hydrogen
lpm	Litre Per Minute
kg	Kilogram
m^3	Cubic Meter
MJ	Mega Joule
cSt	Centistokes
CH_3OH	Methanol

1. Introduction

The efficiency of transportation networks plays a crucial role in a nation's economic development and competitiveness on a global scale [1]. Economic growth depends on increased trade, efficient distribution of goods and services, a thriving tourism sector, and workforce mobility—all of which require a well-developed transportation infrastructure. However, the transportation sector is also one of the largest energy consumers worldwide, accounting for 20–30 % of total energy consumption, depending on the country. In the United States, for example, transportation contributed approximately 27 % of total energy consumption in 2022 [2]. Energy consumption in transportation is a major concern for sustainable energy transitions, as it is primarily met through fossil fuel use in internal combustion engines (ICEs). Emissions from ICEs contribute to air pollution and climate change [3–5]. In response, some governments introduced plans to ban diesel vehicles in major cities, demonstrating a commitment to reducing fossil fuel reliance and promoting alternative energy sources [6,7]. Despite these efforts, the accelerating pace of climate change has revealed that current targets, including those set by the Intergovernmental Panel on Climate Change, are insufficient. As a result, researchers have prioritized the development of alternative energy sources and clean fuel technologies.

In the past decade, hydrogen-based combustion has emerged as one of the most promising methods to enhance engine performance while reducing emissions [8–11]. Several key advantages make hydrogen an attractive alternative fuel: *Zero emissions* – Hydrogen combustion produces only water vapor, eliminating harmful pollutants [8]. *Higher energy efficiency* – Its superior calorific value enhances energy efficiency [12]. *Improved engine performance* – Hydrogen's low ignition energy and high flame speed contribute to more efficient combustion [13]. However, hydrogen storage presents a significant challenge [14]. Hydrogen can be stored as a compressed gas or in liquid form, but both methods have their own limitations related to high costs, safety concerns, and technical feasibility. Furthermore, integrating hydrogen into existing fuel infrastructure requires substantial investments and technological innovations. To address hydrogen storage challenges, onboard hydrogen production in ICEs has emerged as a promising alternative. One potential solution is hydrogen production from methanol and water. Historically, industrial methanol production relied on fossil fuels, raising concerns about greenhouse gas emissions. However, recent advancements in renewable energy sources and carbon capture technologies have made sustainable methanol production increasingly viable [15–17]. In fact, studies predict that renewable methanol could reach price parity with fossil-derived methanol by 2030 [17].

Methanol, often referred to as a hydrogen carrier, enables efficient storage and on-demand reforming, making it an attractive option for onboard hydrogen production [18]. Among various reforming methods methanol steam reforming (MSR) is the most suitable option for ICE applications due to its high hydrogen yield, and optimal H_2/CO ratio [19,20]. Unlike ethanol or methane reforming, which require temperatures above 400–500 °C, MSR operates efficiently at lower temperatures (200–300 °C), making it more practical for use with ICEs [21,22].

In ICEs, a large portion of the fuel energy–approximately 30-40 %–is lost as waste heat through exhaust gases. The exact percentage varies depending on factors such as engine type, design, age, maintenance status, fuel type, ambient temperature, and load conditions [19,23–25]. Therefore, the use of waste heat not only contributes to fuel savings by reducing the need for additional energy but also contributes to a more sustainable hydrogen production. The recent studies in the literature on hydrogen production and analysis by MSR are given below.

In a study by Bayramoğlu [26], the effects of exhaust waste heat on hydrogen production efficiency were investigated numerically. Using Computational Fluid Dynamics (CFD) methods, the study analyzed heat transfer, hydrogen, CO, and CO_2 formation in the MSR reactor were analyzed by for each load condition. In the study, the amounts of hydrogen, CO, and CO_2 formation in the MSR reactor under different load conditions. The results indicated that hydrogen production increases with increasing temperature and catalyst usage, with the maximum hydrogen production mass flow rate reaching approximately 7020 g/h at 25 % engine load condition. Zhao et al. [27] developed a comprehensive model, including a kinetic model, to simulate the conversion and utilization of solar energy in photothermal reactors. Furthermore, they implemented an integrated evaluation system using Taguchi design, ANOVA, and grey relational analysis methods to optimize methanol conversion, hydrogen yield, and CO selectivity. The optimized parameters resulted in a methanol conversion rate of 99.99 %, a hydrogen yield of 3.196 %, and the lowest CO selectivity of $1.71x10^{-3}$. In another work, Chen et al. [28] explored the application of $CuGa_2O_4$ spinel catalyst for low-temperature methanol vapor reforming. Their findings revealed that the catalyst surface consists of highly porous, interconnected particle chains, contributing to an impressive gas selectivity of 98 % for hydrogen and 0.0 % for CO. Additionally, the catalyst demonstrated exceptional durability, showing no deactivation over 50 h.

Huang et al. [29] investigated the effect of various Al_2O_3 precursors and the catalytic performances of Cu/ZnO/Al_2O_3 catalysts in MSR. Their findings showed that the precursor selection significantly affected the precipitation process and, consequently, catalytic efficiency. The study reported a methanol conversion rate of 94.8 % and an H_2 time-space yield of 97.5 mol kg^{-1} h^{-1} at an H_2O/MeOH mole ratio of 1.2 and a temperature of 493 K. Achomo et al. [30] compared the catalytic performance of Cu/ZnO/Al_2O_3 catalysts synthesized by three different methods (coprecipitation, hydrothermal, and sol-gel). The study analyzed the physicochemical, morphological, and thermal properties of these catalysts. The highest methanol conversion (91.5 %) and H_2 yield (90.9 %) at 280 °C were achieved using the coprecipitation method, with a low CO selectivity of 0.61 %. On the other hand, the catalysts synthesized via hydrothermal and sol-gel methods showed significantly lower methanol conversion (39.2 % and 73.5 %) and H_2 yields (39.0 % and 72.7 %), with CO selectivity values of 1.46 % and 0.91 %, respectively. In another study, Alfuhaid et al. [31] explored the use of red mud, an industrial waste material, as a cost-effective and efficient catalyst for steam conversion of diesel fuel into hydrogen. Nickel was impregnated into the red mud at different concentrations, significantly enhancing the water-gas conversion process and achieving three times higher hydrogen selectivity compared to pure red mud. Their results showed that a 20 % Ni-loaded catalyst produced hydrogen with high selectivity (up to 75 %), while maintaining very low selectivity for CO_2, CH_4, and CO. Additionally, the catalyst exhibited stable performance over 20 h. Finaly, Ağbulut et al. [32] designed a thermodynamic equilibrium reactor to analyze the impact of reaction temperature (RT: 100–500 °C), reactor pressure (RP: 1–7 atm), and methanol-to-water ratio (MtW: 0.25, 0.5, 1, 2 and 4) on synthesis gas composition. The authors employed

Table 1
Technical specification of heat source.

Model	Lombardini LDW 1003
Total cylinder volume	1028 cm^3
Maximum power	19.5 kW
Maximum speed	3600 rpm
Maximum torque @2000 rpm	67 Nm

Pareto-based multi-objective evolutionary algorithms (MOEAs) including Improved Multi-Objective Manta-Ray Foraging Optimization (IMOMRFO), Multimodal Multi-Objective Differential Evolution with Improved Crowding Distance (MMODE_ICD), and Multi-Objective Slime Mould Algorithm (MOSMA). Through optimization, the highest hydrogen content obtained was 67.90 %, which could be increased by 7.22 % with MMODE_ICD.

The literature review highlights that a substantial portion of the energy in ICEs is lost as waste heat, particularly through the exhaust manifold. However, research specifically focusing on harnessing this waste heat for hydrogen production in engines remains limited.

In this framework, the present research aims to produce hydrogen-rich synthesis gas (syngas) with high energy density by leveraging waste heat from ICEs. As a key innovation, this study focuses on maximizing the hydrogen content in syngas by optimizing operational parameters using DSC-MOPSO, MOSPO, and MOGWO algorithms.

This objective is achieved through a three-stage approach:

1. **Engine Testing:** The test engine is operated at different load conditions (15, 30, 45, and 60 Nm) at a constant speed of 2000 rpm. Four different fuel types are tested, and the exhaust gas temperature under each operational condition is recorded.
2. **MSR Unit Design:** Using the recorded exhaust gas temperature data, an MSR unit is designed in the Aspen Plus environment. Various methanol-water molar ratios (0.5, 1, 1.5, and 2) are considered, and the synthesis gas composition (H_2, CO_2, CO, MeOH, and H_2O) is determined.
3. **Multi-Objective Optimization:** Finally, efforts are made to maximize the hydrogen content in the produced synthesis gas (syngas) using recently introduced state-of-the-art multi-objective optimization algorithms including Dynamic Switched Crowding-based Multi-Objective Particle Swarm Optimization (DSC-MOPSO) [33], Multi-Objective Stochastic Paint Optimizer (MOSPO) [34], and Multi-Objective Grey Wolf Optimizer (MOGWO) [35].

2. Methodology

2.1. Waste heat source and experimental data collection

In this work, hydrogen-rich syngas is produced via the steam reforming method, which uses methanol and water as hydrogen sources. This system requires an external heat source to initiate hydrogen production. The present work intends to harness waste heat from a three-cylinder, indirect-ignition diesel engine as the heat source. The key technical specifications of this engine are given in Table 1.

Engine tests were conducted under an ambient temperature of 23 °C (±2 °C). In parallel, test fuels were prepared and stored in the Fuel Preparation Laboratory under the same conditions. During testing, the crankshaft was operated at a constant speed of 2000 rpm. A 22-kW dynamometer was employed to vary the engine load from 15 to 60 Nm while maintaining a constant speed. To ensure repeatability and measurement reliability, the engine oil temperature was allowed to reach 50 °C before collecting experimental data for each fuel. Engine speed and torque values were recorded magnetically using a Kistler

Table 2
Sensitivity and ranges of the instruments used in the experiments.

Instrument	Range	Sensitivity
Thermocouple	0–1200 °C	1 °C
Torque meter	0-100 Nm	0.05 Nm
Fuel flow rate	0–100 mL	1 mL
Hydrogen flow rate	0-250 lpm	0.1 lpm
Engine speed	0–5000 rpm	1 rpm

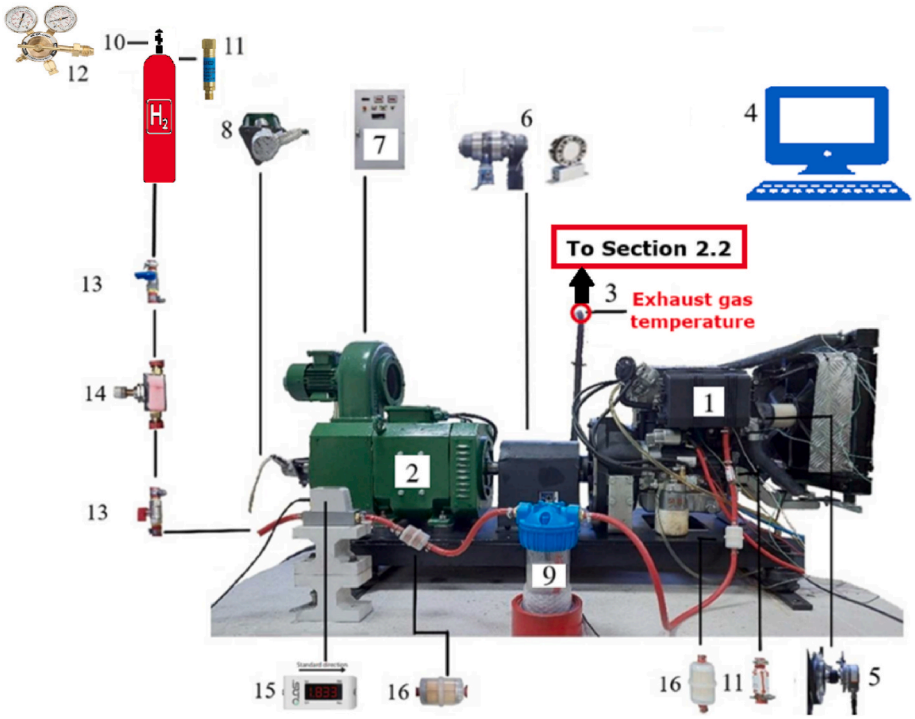

Fig. 1. Experimental rig of the test engine.

Table 3
Test fuel properties.

Test fuel	Density, kg/m^3 at 15 °C	Calorific value, MJ/kg	Cetane number	Viscosity, cSt @ 40 °C
D100	835	42.3	54	2.84
B25	850	41.6	50	3.12
Hydrogen gas	0.08	120.0	–	–
B25 + 15 lpm H_2	–	44.0[c]	–	–
B25 + 30 lpm H_2	–	46.7[c]	–	–

4550A-brand sensor with an accuracy of 0.05 Nm and 1 rpm, directly from the crankshaft. Exhaust Gas Temperature (EGT) values were measured approximately 500 mm from the exhaust manifold through a Ni/Cr-coated K-type thermocouple, which has a measurement range of 0–1000 °C with an accuracy of 1 °C. Additionally, hydrogen flow rates were recorded using a SUTO S418 thermal mass flowmeter, with an accuracy of 1.5 %, based on the DIN1343 standard. The experimental rig setup is illustrated in Fig. 1, and details of the experimental equipment used in this study are given in Table 2.

In this study, the engine was operated using various fuel blends. The first fuel was 100 % conventional diesel (D100), supplied by a commercial company. The second fuel blend, B25, consisted of 75 % diesel fuel and 25 % waste oil biodiesel (by volume). Additionally, hydrogen gas at flow rates of 15 and 30 lpm was mixed with fresh air when the engine was fueled with B25. The properties of these fuels are summarized in Table 3.

2.2. Design of hydrogen production unit

This paper focuses on producing hydrogen-rich gas using the MSR process, based on the Gibbs energy minimization method. The thermodynamic system is modeled in *Aspen Hysys* under chemical equilibrium conditions, utilizing the Peng-Robinson equation of state to calculate the physicochemical properties of the reactants under varying operation conditions. In this study, methanol and water are used as liquid-phase reactants and hydrogen carriers, both starting at initial conditions of 25 °C and 1 atm. Methanol offers significant advantages as an alcohol for systems utilizing waste heat. For instance, its reforming temperature is relatively low compared to natural gas, biogas, ethanol, and ammonia [32,36]. Moreover, its storage is easy at atmospheric conditions [37,38].

The reactants are mixed using a two-way inlet and single-way outlet mixer. The resulting mixture was transferred to a heat exchanger using a pump with an adiabatic efficiency of 75 %. At this stage, the temperature of the mixture is raised to 100 °C, converting it completely from liquid to vapor.

Subsequently, the methanol-water stream is directed into an equilibrium reactor via a compressor with an isentropic efficiency of 75 %. The reactor, modeled in a vertical cylindrical geometry with a height of 1 m and a diameter of 0.5 m (≈0.2 m^3), operates under chemical equilibrium. The primary components within the reactor include hydrogen (H_2), carbon monoxide (CO), carbon dioxide (CO_2), water (H_2O), and methanol (MeOH), as determined in the simulation. The MSR unit modeled in this study is illustrated in Fig. 2.

During the analysis of the waste-heated MSR unit designed in this work, the following assumptions were made to achieve the results:

- **Steady-State and Equilibrium Conditions:** The waste-heated MSR unit operates at steady-state and thermodynamic equilibrium conditions. All components in the streams exhibit Peng-Robinson state characteristics.
- **Constant Input Conditions:** Methanol and water have constant temperature and pressure values when entering the system, with any impurities in the reactants neglected.
- **No Pre-Reaction:** The hydrogen carriers do not react with each other before entering the equilibrium reactor.
- **Uniform Conditions:** Temperature and pressure distribution are uniform in all components of the waste-heated MSR unit, and the modeled system is perfectly adiabatic with no heat loss to the environment.

2.3. Multi-objective optimization algorithms

This study employed recently developed robust Pareto-based multi-objective optimization techniques to maximize the hydrogen content in the produced syngas. To achieve this, the dynamic switched crowding-based multi-objective particle swarm optimization (DSC-MOPSO), multi-objective stochastic paint optimizer (MOSPO), and multi-objective grey wolf optimizer (MOGWO) are employed. The following subsections provide a brief introduction to the multi-objective optimization algorithms used in this study.

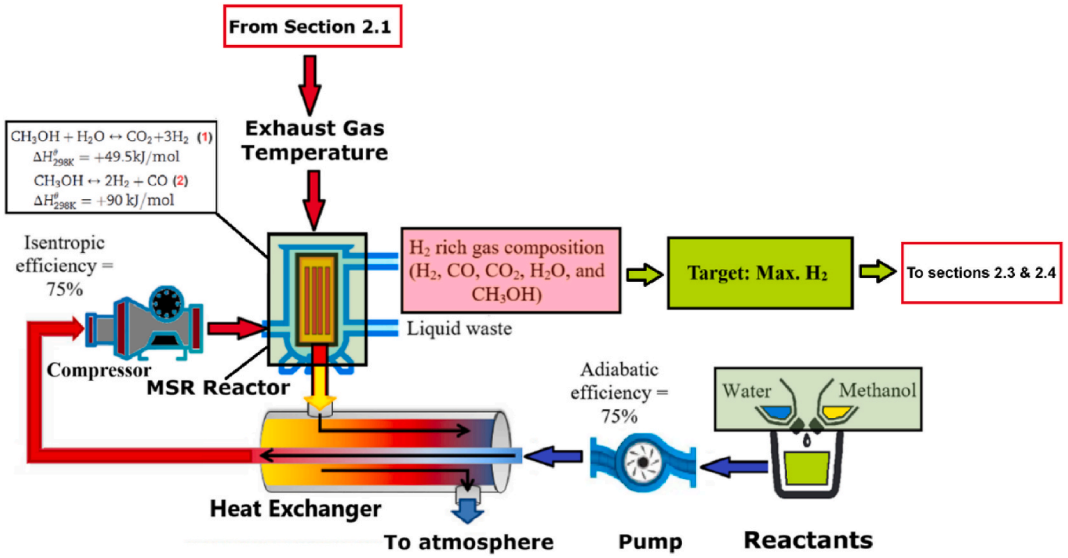

Fig. 2. Waste heated-methanol steam reforming unit.

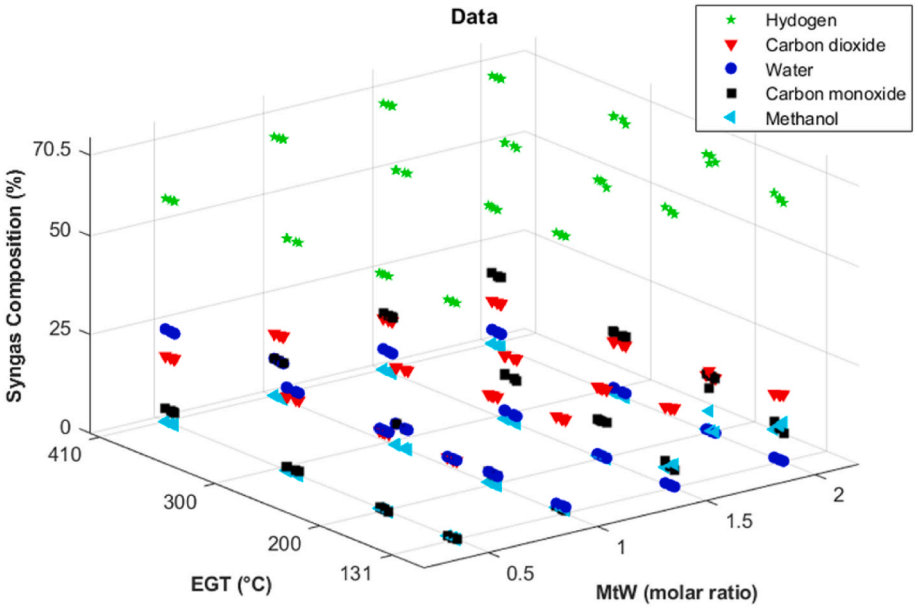

Fig. 3. Visual representation of measured data.

2.3.1. Dynamic switched crowding-based multi-objective particle swarm optimization (DSC-MOPSO)

DSC-MOPSO [33] is a recently developed state-of-the-art evolutionary optimization technique specifically designed to handle multi-objective optimization problems, where multiple conflicting objectives must be optimized simultaneously. The algorithm effectively balances these objectives, identifying a set of non-dominated solutions that provide an optimal trade-off between competing criteria. The optimization framework of DSC-MOPSO consists of three key stages. These are Pareto-based archiving, dynamic switched crowding-based archive handling [39], and particle swarm optimization (PSO)-based metaheuristic search process [40]. For detailed information on the DSC-MOPSO algorithm, please refer to the original study by Bakır et al. [33].

2.3.2. Multi-objective stochastic paint optimizer (MOSPO)

MOSPO [34] is an innovative meta-heuristic optimization algorithm inspired by color theory and painting techniques. It is an efficient variant of the single-objective stochastic paint optimizer (SPO) [41], adapted to handle multi-objective optimization problems. MOSPO incorporates several enhancements including archive, leader selection, and grid mechanism. The algorithm stores non-dominated solutions found during the optimization process with a Pareto-based archiving mechanism. The selection of leaders from the archive helps to guide the search towards promising regions of the solution space. The grid mechanism plays an important role in effectively managing the archive and increasing exploration. By incorporating these additional features, MOSPO can effectively handle complex multi-objective optimization problems and generate a diverse set of high-quality solutions. Further information about the MOSPO algorithm can be found in the original study by Khodadadi et al. [34].

2.3.3. Multi-objective grey wolf optimizer (MOGWO)

MOGWO [35] is a well-known multi-objective optimization technique derived from the single-objective grey wolf optimizer (GWO) [42]. To adapt GWO to handle multiple conflicting objectives, MOGWO incorporates two key components: Pareto-based archiving and leader selection strategy. MOGWO simulates the social hierarchy of grey wolves, with alpha, beta, and delta wolves leading the pack in the metaheuristic search process. The social hierarchy and hunting mechanisms (encircling prey, hunting, and attacking) ensure a good balance between global exploration and local exploitation. MOGWO has gained significant attention from the research community since its introduction. Its strong performance and relatively simple implementation have made it a popular choice for solving a wide range of multi-objective optimization problems. More information on the optimization process of MOGWO can be found in the original study by Mirjalili et al. [35].

2.4. Modelling of multi-objective optimization process

The present work aims to investigate the hydrogen production potential of an MSR reactor. Accordingly, in the experiments, three-cylinder, water-cooled, and indirect ignition diesel engine is run at varying engine loads and constant engine speeds. The system designed used the waste heat released to the atmosphere from the test engine. Then, the results are optimized by using DSC-MOPSO, MOSPO, and MOGWO algorithms, aiming to maximize the hydrogen composition at the outlet of the reactor. In the study, hydrogen (f_{H_2}), carbon dioxide (f_{CO_2}), water (f_{H_2O}), carbon monoxide (f_{CO}), and methanol (f_{MeOH}) amounts in syngas composition were selected as objective functions, and the best settings of input parameters (EGT and MtW) to optimize these objectives were investigated. The objective functions are described in Equation (1).

$$\text{Objective functions}\begin{cases}\max OF_1 = f_{H_2}\\ \min OF_2 = f_{CO_2}\\ \min OF_3 = f_{H_2O}\\ \min OF_4 = f_{CO}\\ \min OF_5 = f_{MeOH}\end{cases} \tag{1}$$

As can be seen in Equation (1), multi-objective optimization aims to maximize the amount of hydrogen while minimizing the amount of other gases. To find the Pareto-optimal solution set that can well balance five objectives, multi-objective optimization was performed with DSC-MOPSO, MOSPO and MOGWO algorithms. The mathematical models of the objective functions are derived from response surface methodology (RSM) analysis [43–45] using the data shown in Fig. 3. Accordingly, a regression model between optimization objectives and input parameters was fitted and presented in Equations (2)–(6).

$$f_{H_2} = 0.738 + 0.000146 \times \text{EGT} - 0.0291 \times \text{MtW} - 0.000001 \times \text{EGT}^2 - 0.0223 \times \text{MtW}^2 + 0.000313 \times \text{EGT} \times \text{MtW} \tag{2}$$

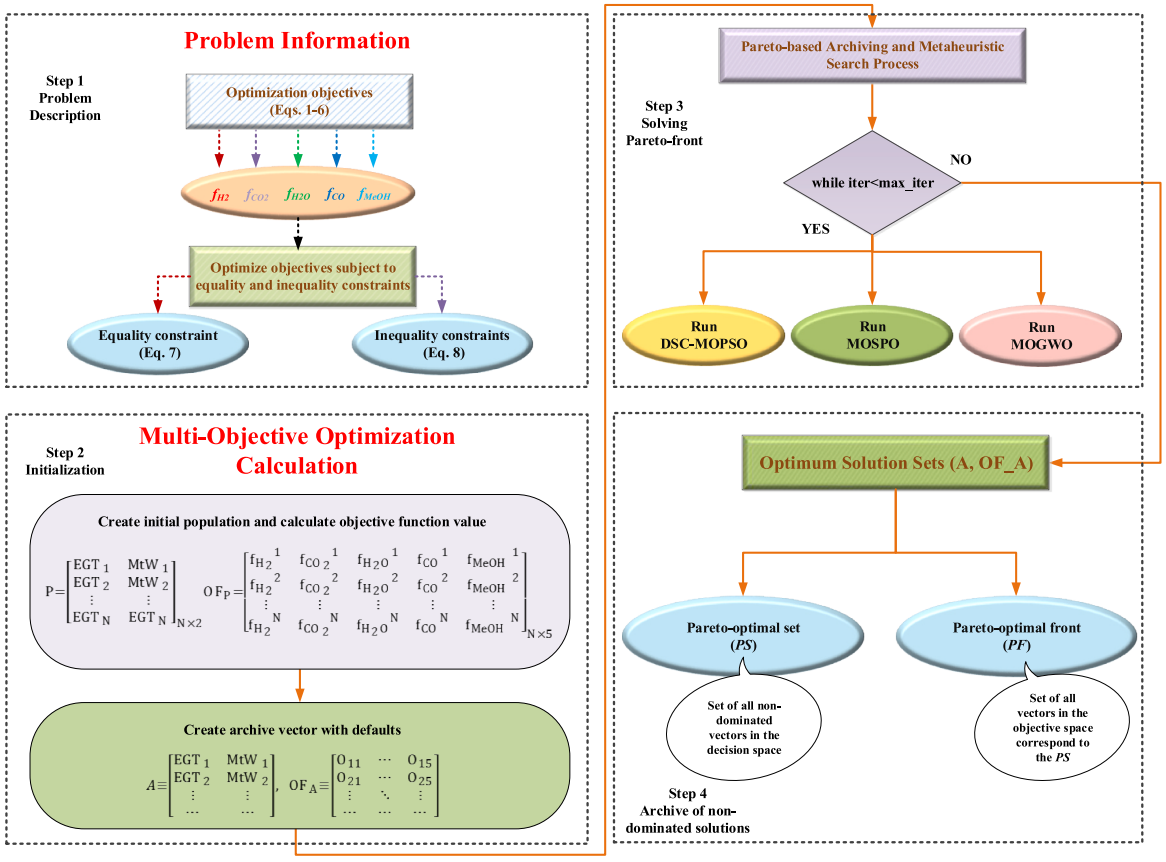

Fig. 4. Flowchart of multi-objective optimization process with Pareto-based algorithms.

$$f_{CO_2} = 0.4033 - 0.00038 \times \mathrm{EGT} - 0.1403 \times \mathrm{MtW} + 0.01644 \times \mathrm{MtW}^2 + 0.000094 \times \mathrm{EGT} \times \mathrm{MtW} \tag{3}$$

$$f_{H_2O} = 0.07726 + 0.000169 \times \mathrm{EGT} - 0.11012 \times \mathrm{MtW} + 0.000001 \times \mathrm{EGT}^2 + 0.03936 \times \mathrm{MtW}^2 - 0.000163 \times \mathrm{EGT} \times \mathrm{MtW} \tag{4}$$

$$f_{CO} = -0.236 + 0.000643 \times \mathrm{EGT} + 0.1959 \times \mathrm{MtW} - 0.000001 \times \mathrm{EGT}^2 - 0.0358 \times \mathrm{MtW}^2 + 0.000015 \times \mathrm{EGT} \times \mathrm{MtW} \tag{5}$$

$$f_{MeOH} = 0.0174 - 0.000577 \times \mathrm{EGT} + 0.0836 \times \mathrm{MtW} + 0.000001 \times \mathrm{EGT}^2 + 0.0023 \times \mathrm{MtW}^2 - 0.000259 \times \mathrm{EGT} \times \mathrm{MtW} \tag{6}$$

The objective functions described in Equation (1) should be optimized subject to various equality and inequality constraints. The sum of the amounts of the syngas composition components should be equal to 1 mol. This represents the equality constraint of the problem and can be written as in Equation (7). The limits of the decision variables given in Equation (8) represent the inequality constraint of the problem.

$$f_{H_2} + f_{CO_2} + f_{H_2O} + f_{CO} + f_{MeOH} = 1 \tag{7}$$

$$\text{Decision variables} = \begin{cases} 131 \le \mathrm{EGT} \le 410 \\ 0.5 \le \mathrm{MtW} \le 2.00 \end{cases} \tag{8}$$

The settings followed in the experimental studies regarding multi-objective optimization are as follows: the maximum number of iterations is 100, the population and maximum archive size are equal and its value is 200. Fig. 4 shows the flowchart of a multi-objective optimization study with DSC-MOPSO, MOSPO, and MOGWO algorithms. The optimization steps in the figure are explained in detail below:

Step 1-Poblem Description: The first step includes defining the mathematical model of the optimization problem. The objective functions of the hydrogen content maximization problem are defined in Equations (1)–(6), and the equality and inequality constraints of the problem are given in Equations (7) and (8).
Step 2-Initialization: In this step, population (*P*) and archive (*A*) vectors are created based on the defaults of the optimization problem. The objective function values of the solution candidates in the *P*-population and the non-dominated solutions in the *A*-archive are stored in the OF_P and OF_A vectors, respectively.
Step 3-Solving Pareto-Front: The third step covers the crowding distance-based Pareto archiving and metaheuristic search process to obtain Pareto-optimal solution sets. In this direction, archive update, crowding distance-based ranking, archive handling and metaheuristic search with exploration and exploitation operators are conducted for DSC-MOPSO, MOSPO, and MOGWO algorithms. The operations of Step 3 are continued until the stopping criterion is met.
Step 4-Archive of Non-Dominated Solutions: In the last step of the optimization process, the non-dominated solution vectors in the decision and objective spaces are archived in *PS* and *PF* vectors, respectively. In the hydrogen content maximization problem, the optimal values of the decision variables (EGT and MtW) are selected from the *PS* vector and the corresponding objective function values ($f_{H_2}, f_{co_2}, f_{H_2O}, f_{CO}, f_{MeOH}$) are selected from the *PF* vector.

3. Result and discussion

This section consists of three main parts. First, the diesel engine's

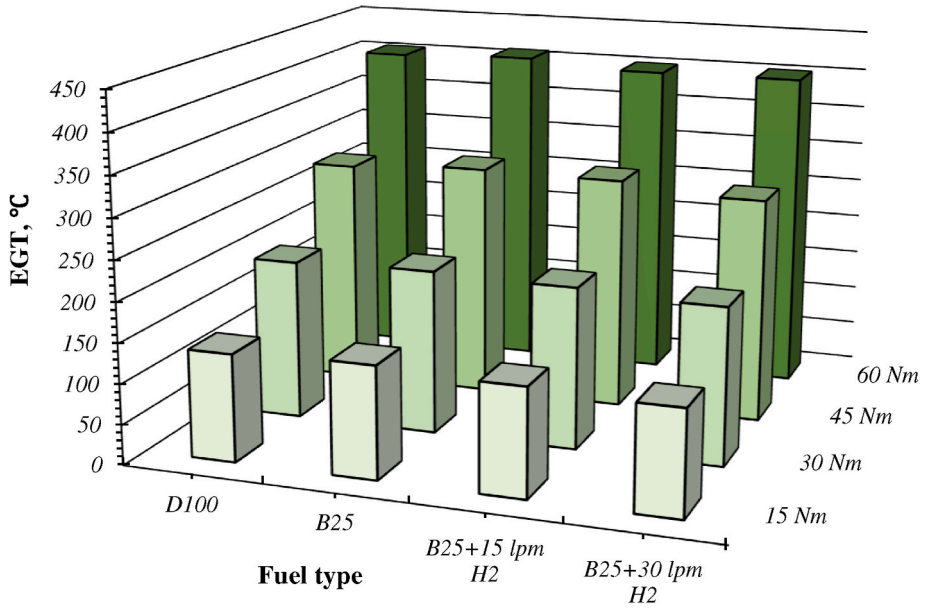

Fig. 5. Exhaust gas temperature at varying engine loads.

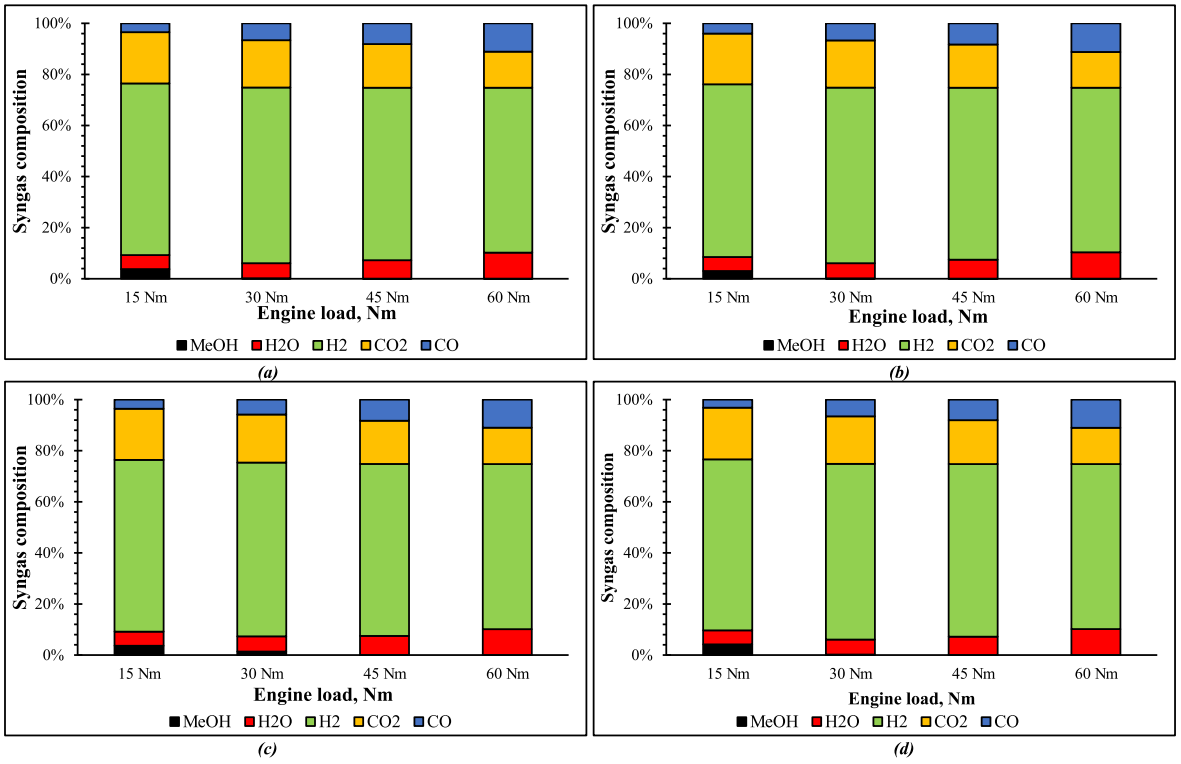

Fig. 6. Syngas composition at the outlet of the reactor a) D100, b) B25, c) B25 + 15 lpm, and d) B25 + 30 lpm.

exhaust gas temperature (EGT) data for different engine loads and fuel types will be analyzed. In the next subsection, a methanol steam reformer unit will be modeled based on these exhaust gas temperatures, considering different methanol-water molar ratios, to evaluate the usability potential of waste heat for syngas production. Finally, the parameters from the previous two subsections will be optimized using three novel algorithms to maximize the hydrogen amount in the produced syngas.

3.1. Exhaust gas temperature

Fig. 5 presents the EGT values for the engine operating under different load conditions. As shown in the figure, EGT values increase as the engine increases for all test fuels. This is because, at higher loads, the engine requires more fuel to maintain the same speed, resulting in higher fuel combustion rates and consequently higher EGT values.

The EGT value is influenced by both the physical and chemical properties of fuel mixtures and engine operating conditions. Specifically, the calorific value of the fuel and the combustion rate

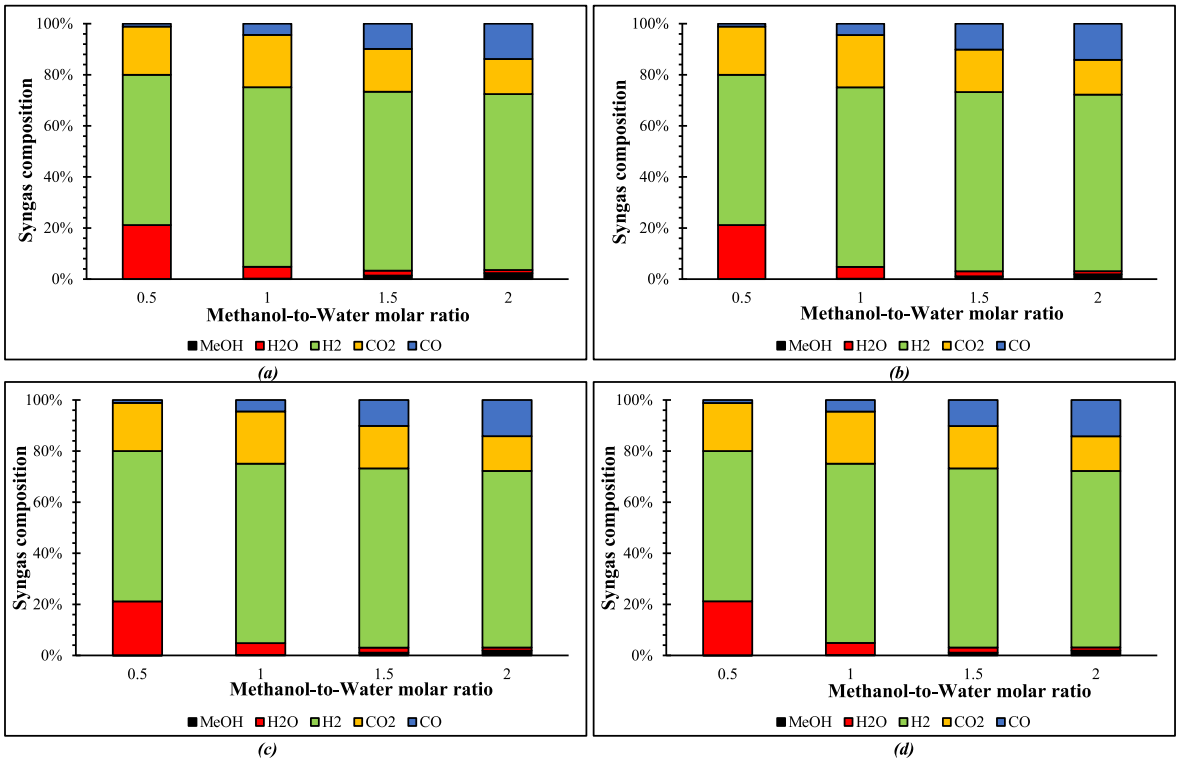

Fig. 7. Syngas composition at the outlet of the reactor a) D100, b) B25, c) B25 + 15 lpm, and d) B25 + 30 lpm.

Table 4
Comparative optimization results.

Algorithm	Design parameters		Objectives				
	EGT (°C)	MtW(molar ratio)	f_{H_2} (%)	f_{CO_2} (%)	f_{H_2O} (%)	f_{CO} (%)	f_{MeOH}(%)
DSC-MOPSO	193.31	1.532	72.5	18.1	2.3	7.1	0.0
MOSPO	195.73	1.568	72.4	17.8	2.3	7.5	0.0
MOGWO	203.80	1.691	72.1	16.8	2.3	8.8	0.0

significantly affect the EGT measurements. The thermocouple used for EGT measurement was installed approximately 50 cm from the engine exhaust pipe. Therefore, if combustion is delayed due to incomplete combustion in the combustion chamber, the EGT value may increase as more fuel continues to burn in the exhaust phase. The average EGT values recorded for all loads were 256, 262.25, 257.75, and 252.75 °C for D100, B25, B25 + 15H_2, and B25 + 30H_2 fuels, respectively. Each experiment was repeated three times under the same conditions for all test fuels, and the obtained data were averaged, with error margins between 0.244 % and 0.763 %. With B25, which has the smallest calorific value (see Table 2), the largest average EGT value was obtained for all loads. This can be attributed to the higher specific fuel consumption value of B25 compared to D100, the higher latent heat of vaporization of B25, and the lower cetane number of B25 [46].

Due to its lower cetane number, B25 has a longer ignition delay compared to D100, causing more fuel to accumulate in the cylinder before combustion occurs. This leads to higher combustion temperature and shifts part of the combustion process into the exhaust phase, resulting in increased EGT values.

Furthermore, hydrogen's high calorific value (Table 3) significantly impacts post-combustion temperature [47]. The calorific values for B25 + 15H_2 and B25 + 30H_2 fuels were calculated and are given in Table 2. The addition of H_2 to B25 increased the average calorific value of the fuel blend. Since less B25 was required to produce the same engine torque, the specific fuel consumption decreased. In addition, hydrogen's high flame speed shortened the combustion duration, preventing combustion from extending into the exhaust phase, which ultimately lowered the EGT values for B25 blends with H_2.

For these reasons, although B25 + 30H_2 has the highest calorific value, it exhibits the lowest average EGT values across all load conditions. The results indicate that combustion with B25 + 30H_2 was completed more quickly, leading to the highest combustion efficiency. Consequently, a greater portion of the combustion energy was effectively converted into useful work, reducing heat loss through exhaust.

3.2. Hydrogen-rich gas production

Fig. 6 shows the impact of engine load on the syngas composition. In the methanol steam reforming (MSR) process, syngas composition varies significantly due to the thermodynamic and enthalpy properties of the reactants, which strongly depend on the reaction temperature. From the figure, it is evident that the hydrogen content is the highest among all gas components at any given engine load.

When comparing hydrogen percentages, the maximum hydrogen yield is consistently obtained when the engine operates at 30 Nm for all fuels. Numerically, the hydrogen content in syngas ranges from approximately 68.1 to 68.8 % at 30 Nm with reactor temperature recorded as 200, 205, 202, and 196 °C for D100, B25, B25 + 15 lpm H_2, and B25 + 30 lpm H_2, respectively. Methanol, unlike other hydrocarbons, lacks carbon-carbon bonds, meaning it requires less energy for decomposition. As a result, these temperatures are considered relatively low for any steam reforming process [32,48,49].

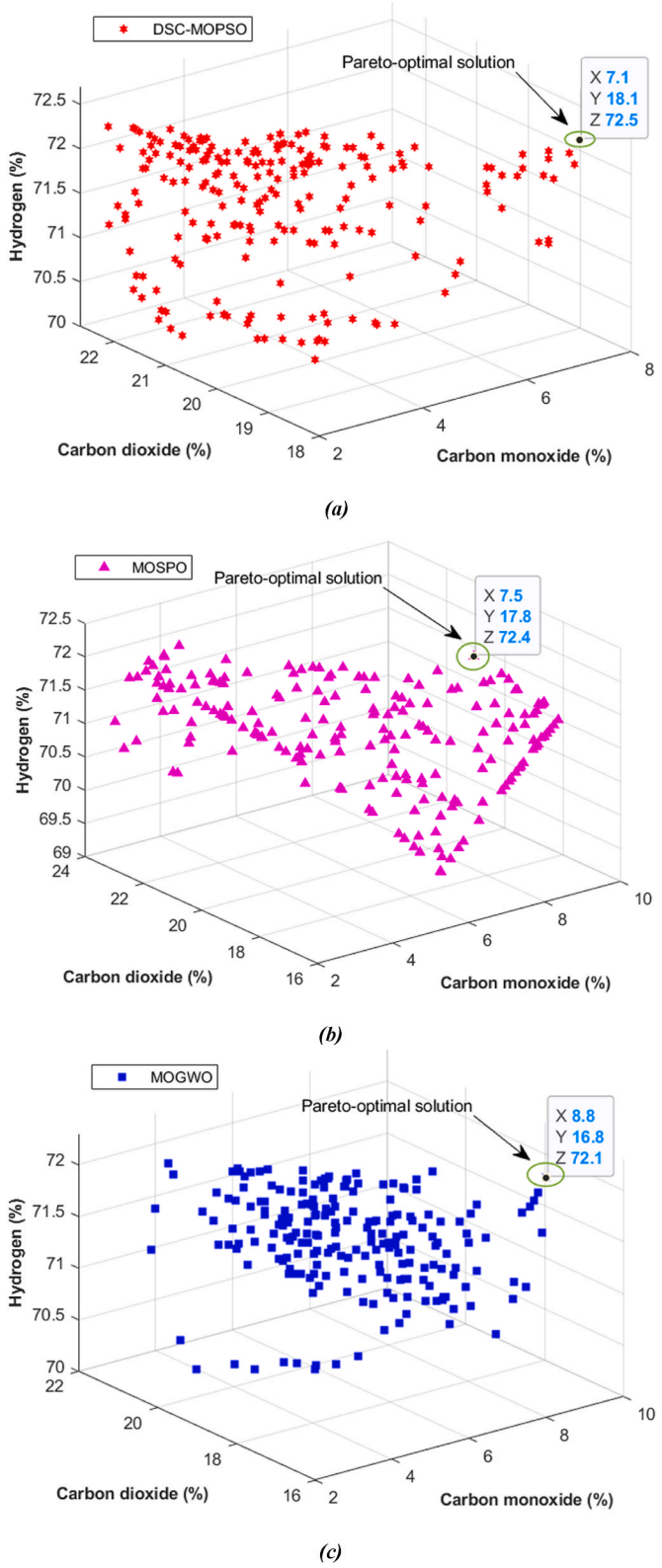

Fig. 8. Pareto optimal frontier formed by multi-objective optimizers: a) DSC-MOPSO, b) MOSPO, and c) MOGWO.

Another key observation from Fig. 6 is the gradual decrease of unreacted methanol percentage as engine load increases. The main MSR reaction ($CH_3OH + H_2O \rightarrow CO_2 + 3H_2$) is endothermic, and methanol decomposition via the side reaction ($CH_3OH \rightarrow CO + 2H_2$) is limited at lower temperatures. Consequently, as seen in Fig. 6, the highest percentage of unreacted methanol appears at 15 Nm engine load, where the lowest temperatures are recorded. However, even at this low load, the unreacted methanol percentage remains below 0.5 %. At 30 Nm engine load, as temperature rises, the unreacted methanol percentage drops below 0.02 % for all test fuels. Beyond this load, no detectable unreacted methanol remains in the syngas, indicating a methanol conversion rate exceeding 99.9 % for all test fuels when the engine load exceeds 30 Nm.

Additionally, an inverse correlation between CO_2 and CO formations is observed in Fig. 6. As the engine load increases, CO_2 concentration gradually decreases, while CO concentration increases. Since higher engine loads correspond to higher temperatures, the CO formation increases as the side reaction producing CO is endothermic, meaning more CO is generated at elevated temperatures.

Although side reactions in the MSR process are generally undesirable, the increase in temperature enhances methanol decomposition, leading to higher CO formation. This trend further suggests that the primary reaction ($CH_3OH + H_2O \rightarrow CO_2 + 3H_2$) occurs less frequently at higher temperatures, explaining the decrease in CO_2 levels while CO levels rise.

Fig. 7 shows the syngas composition as a function of methanol-to-water (MtW) molar ratio. As can be seen in the figure, gas composition depends strongly on the MtW molar ratio and changes significantly as this ratio changes. Most importantly, the lowest hydrogen content is observed at MtW molar ratio of 0.5, averaging 59.8 %. At this ratio, the methanol concentration in the reactant mixture is too low, which slows down the steam-reforming reactions, reducing the overall reaction conversion efficiency. As a result, the H_2 yield in the system decreases, limiting hydrogen production in the MSR process.

On the other hand, the methanol content should not be excessively high in the MtW mixture. Excess methanol leads to an increase in unreacted MeOH in the syngas and promotes side reactions, particularly: ($CH_3OH \rightarrow CO + 2H_2$). This explains why, as the MtW ratio increases, CO concentrations in the syngas composition also increase (see Fig. 7). The highest H_2 yield is achieved at an MtW molar ratio of 1, where H_2 constitutes 70.3 % of the total syngas composition, considering all test fuels collectively. Another key observation from Fig. 7 is the high H_2O content in syngas at an MtW molar ratio of 0.5, which correlates with poor H_2 formation across all test fuels. At this ratio, the water content in syngas exceeds 20 % for each test fuel. This occurs because the methanol and water proportions are far from the optimal ratio, leading to an excess of unreacted water in the system. However, as the MtW ratio increases, the water content in syngas significantly decreases: 4.64 % at an MtW ratio of 1, 1.96 % at an MtW ratio of 1.5, and 1.23 % at an MtW ratio of 2. This trend indicates that higher MtW ratios promote more efficient water utilization, leading to a greater conversion of water into hydrogen in the reforming process.

3.3. Optimization results

Table 4 shows the optimal design variable settings and the corresponding objective function results obtained using the DSC-MOPSO, MOSPO, and MOGWO algorithms. As per the results, the DSC-MOPSO algorithm achieved the highest hydrogen content, reaching 72.5 % (see Fig. 8). This optimal result was obtained at an EGT of 193.31 °C and an MtW molar ratio of 1.532. The MOSPO algorithm ranked second in hydrogen production performance, yielding 72.4 % hydrogen content. The Pareto-optimal solution for MOSPO was found at an EGT of 195.73 °C and an MtW molar ratio of 1.568. Meanwhile, the MOGWO algorithm produced a slightly lower hydrogen content, which was 0.551 % and 0.414 % lower than the DSC-MOPSO and MOSPO results, respectively.

As shown in Table 4, the Pareto-optimal front includes the percentages of hydrogen (f_{H_2}), carbon dioxide (f_{CO_2}), water (f_{H_2O}), carbon monoxide (f_{CO}), and methanol (f_{MeOH}) in the syngas composition. The Pareto front is visualized for hydrogen, carbon dioxide, and carbon

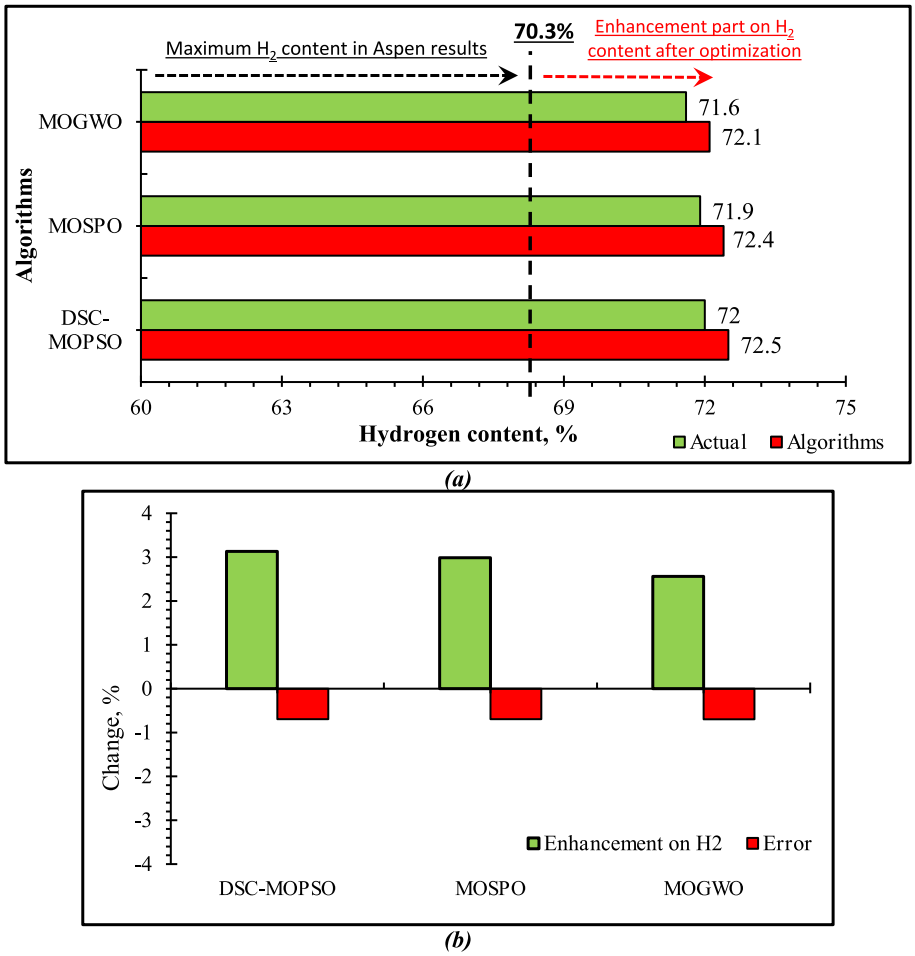

Fig. 9. **(a)** Optimized and actual results, **(b)** enhancement on H_2, and the comparison of the errors.

monoxide, as these components have the highest concentration in the syngas. Fig. 8 shows the Pareto optimal frontier produced by the DSC-MOPSO, MOSPO, and MOGWO algorithms. As observed in the figure, during the optimization process DSC-MOPSO achieves hydrogen content ranging from 70 % to 72.5 %, MOSPO results in hydrogen content between 69 % and 72.4 %, and MOGWO produces hydrogen levels between 70 % and 72.1 %. The numerical results confirm that DSC-MOPSO is a robust and highly efficient optimization method, outperforming the other algorithms in solving the given problem. Fig. 8 also demonstrates that all algorithms successfully generated a diverse and well-distributed Pareto front, indicating effective optimization performance across multiple objectives.

The validation of the optimal operating parameters generated by the multi-objective optimization algorithms for maximizing hydrogen production was conducted in Aspen Plus. The maximum amount of hydrogen obtained under optimal operating conditions in Aspen Plus is given in Fig. 9. As shown in Fig. 9(b), the error between optimization and simulation results is smaller than 0.7 % for all algorithms (*See* Fig. 9 (b)), the error between the optimization results and simulation results is less than 0.7 % for all algorithms. These error values confirm that Pareto-based algorithms demonstrate robust and reliable optimization performance in enhancing hydrogen content in the syngas produced from the MSR unit.

Considering all optimization results, it is evident that DSC-MOPSO outperforms MOSPO and MOGWO. The superior performance of DSC-MOPSO can be attributed to the following key factors:

1. Efficient archive management using the DSC method, which enhances solution diversity and convergence.
2. Guide selection from both population and archive vectors, improving search direction and optimization accuracy.
3. Robust exploration and exploitation operators from PSO, enabling a more effective metaheuristic search process.

These features collectively contribute to the strong optimization performance of DSC-MOPSO, making it more effective than the other algorithms for maximizing hydrogen content in syngas.

4. Conclusions

This research aims to develop an onboard hydrogen-rich syngas production system using a methanol steam reforming (MSR) unit, which utilizes waste exhaust heat from a diesel engine operating under different loads. Furthermore, the study seeks to maximize hydrogen content in syngas by optimizing operational parameters using DSC-MOPSO, MOSPO, and MOGWO algorithms. In conclusion, the following key findings have been drawn from this research:

- Exhaust gas heat in ICEs contains significant energy, but it is typically not utilized in practical applications. This research proves that hydrogen-rich syngas can be effectively produced using EGT at all engine loads tested. Interestingly, H_2 content in syngas is highest at medium engine loads, whereas at very low or very high engine loads, slight decreases in H_2 content occur due to excessively high or low EGT values.
- Syngas composition does not vary significantly based on fuel type; however, engine operating parameters, such as engine speed and

load, have a greater impact on syngas composition than specific test fuel used.
- The MtW molar ratio is the most influential parameter affecting syngas composition. The highest H_2 content is observed when the MtW molar ratio is 1. Deviating from this ratio increases other gas components, leading to a gradual decrease in H_2 content.
- Optimization results indicate that the maximum hydrogen content at the MSR reactor outlet was 72.5 % with DSC-MOPSO, 72.4 % with MOSPO, and 72.1 % with MOGWO.
- The DSC-MOPSO algorithm achieved the highest hydrogen yield at an EGT of 193.31 °C and an MtW molar ratio of 1.532.
- The percentage error between optimization results and Aspen Plus simulations was less than 0.7 %, confirming the accuracy and reliability of the optimization process.
- Hydrogen content increased from 70.3 % to 72.5 % through a multi-objective optimization, representing a 3.13 % improvement in hydrogen yield at the reactor outlet, achieved using DSC-MOPSO.

To summarize, approximately one-third of the fuel energy in ICEs is lost as waste heat through the exhaust manifold, which is directly discharged into the atmosphere without being utilized. This study demonstrates that it is possible to produce onboard hydrogen-rich syngas using an MSR unit powered solely by this waste heat. The findings indicate that H_2 production can be increased by 3.13 % by optimizing key operating parameters.

As a practical application, future research can focus on the feasibility of mixing hydrogen-rich syngas with fresh intake air before introducing it into the combustion chamber. At this stage, the real-time utilization of syngas without storage should be explored, taking into account thermal management and safety precautions. Such an approach would enable the development of an H_2-rich gas production system in the form of a retrofit kit that can be integrated into both gasoline and diesel engines.

This advancement could be highly beneficial in terms of fuel economy, as it would increase the energy density of fuels in the combustion chamber while also reducing environmental impacts. Finally, conducting a comparative analysis of a methanol steam reforming system versus conventional ICEs in terms of thermodynamic efficiency, thermoeconomics, and overall sustainability would provide valuable insights for future research. Further studies are necessary to fully evaluate the practicality and economic feasibility of this approach, contributing to the advancement of clean energy technologies.

CRediT authorship contribution statement

Ümit Ağbulut: Conceptualization, Methodology, Investigation, Formal analysis, Data curation, Writing - original draft. **Petr Vozka:** Conceptualization, Methodology, Investigation, Formal analysis, Data curation, Writing - original draft. **Hüseyin Bakır:** Conceptualization, Methodology, Investigation, Software, Formal analysis, Data curation, Writing - original draft. **Nathan A. Brieu:** Conceptualization, Methodology, Investigation, Formal analysis, Data curation, Writing - original draft. **Fikret Polat:** Conceptualization, Methodology, Investigation, Formal analysis, Data curation, Writing - original draft. **Suat Sarıdemir:** Conceptualization, Methodology, Investigation, Formal analysis, Data curation, Writing - original draft.

Declaration of competing interest

The authors declare that they have no known competing financial interests or personal relationships that could have appeared to influence the work reported in this paper.

Acknowledgements

Ümit Ağbulut was supported by TUBITAK 2219-coded project under Grant Number 1059B192300207. The author thanks TUBITAK for its financial support. *Nathan A. Brieu* is the recipient of a CREST fellowship, for which we are grateful. This work has also been supported by an *NSF HRD-2112554* grant.

References

[1] Magazzino C, Mele M. On the relationship between transportation infrastructure and economic development in China. Res Transport Econ 2021;88:100947.
[2] U.S. Energy Information Administration. Monthly energy review, tables 2.1b, 2.5, 3.7c, 3.8c, 10.2c, 10.3, and 10.4 (a, b, and c). 2022. May 2023, preliminary data for.
[3] Leach F, Kalghatgi G, Stone R, Miles P. The scope for improving the efficiency and environmental impact of internal combustion engines. Transport Eng 2020;1:100005.
[4] Santos NDSA, Roso VR, Malaquias ACT, Baeta JGC. Internal combustion engines and biofuels: examining why this robust combination should not be ignored for future sustainable transportation. Renew Sustain Energy Rev 2021;148:111292.
[5] Fayyazbakhsh A, Bell ML, Zhu X, Mei X, Koutný M, Hajinajaf N, Zhang Y. Engine emissions with air pollutants and greenhouse gases and their control technologies. J Clean Prod 2022;376:134260.
[6] Jonidi Jafari A, Charkhloo E, Pasalari H. Urban air pollution control policies and strategies: a systematic review. J Environ Health Sci Eng 2021;19:1911–40.
[7] Töller AE. Driving bans for diesel cars in German cities: the role of ENGOs and Courts in producing an unlikely outcome. European Policy Anal 2021;7(2):486–507.
[8] Alçelik N, Sarıdemir S, Polat F, Ağbulut Ü. Role of hydrogen-enrichment for indirect diesel engine behaviours fuelled with the diesel-waste biodiesel blends. Energy 2024;302:131680.
[9] Hoang AT, Pandey A, De Osés FJM, Chen WH, Said Z, Ng KH, Nguyen XP. Technological solutions for boosting hydrogen role in decarbonization strategies and net-zero goals of world shipping: challenges and perspectives. Renew Sustain Energy Rev 2023;188:113790.
[10] Shahid MI, Rao A, Farhan M, Liu Y, Salam HA, Chen T, Ma F. Hydrogen production techniques and use of hydrogen in internal combustion engine: a comprehensive review. Fuel 2024;378:132769.
[11] Algayyim SJM, Saleh K, Wandel AP, Fattah IMR, Yusaf T, Alrazen HA. Influence of natural gas and hydrogen properties on internal combustion engine performance, combustion, and emissions: a review. Fuel 2024;362:130844.
[12] Shadidi B, Najafi G, Yusaf T. A review of hydrogen as a fuel in internal combustion engines. Energies 2021;14(19):6209.
[13] Gao J, Wang X, Song P, Tian G, Ma C. Review of the backfire occurrences and control strategies for port hydrogen injection internal combustion engines. Fuel 2022;307:121553.
[14] Hassan Q, Algburi S, Sameen AZ, Jaszczur M, Salman HM. Hydrogen as an energy carrier: properties, storage methods, challenges, and future implications. Environ Syst Decisions 2024;44(2):327–50.
[15] Wei H, Su C, Dai J, Albdeiri MS, Alsenani TR, Elattar S, Hua Y. Towards a sustainable, and economic production future: proposing a new process for methanol production based on renewable hydrogen. J Clean Prod 2023;389:135976.
[16] Chen C, Yang A, Bañares-Alcántara R. Renewable methanol production: understanding the interplay between storage sizing, renewable mix and dispatchable energy price. Adv Appl Energy 2021;2:100021.
[17] Schorn F, Breuer JL, Samsun RC, Schnorbus T, Heuser B, Peters R, Stolten D. Methanol as a renewable energy carrier: an assessment of production and transportation costs for selected global locations. Adv Appl Energy 2021;3:100050.
[18] Farooq MS, Baig A, Wei Y, Liu H, Zeng Z, Shi Z. A comprehensive analysis of a compact-sized methanol cracking unit for hydrogen production. Int J Hydrogen Energy 2024;87:822–37.
[19] Srivastava A, Kumar P, Dhar A. A numerical study on methanol steam reforming reactor utilizing engine exhaust heat for hydrogen generation. Int J Hydrogen Energy 2021;46(76):38073–88.
[20] Wu HW, Hsu TT, Fan CM, He PH. Reduction of smoke, PM2. 5, and NOX of a diesel engine integrated with methanol steam reformer recovering waste heat and cooled EGR. Energy Convers Manag 2018;172:567–78.
[21] Ranjekar AM, Yadav GD. Steam reforming of methanol for hydrogen production: a critical analysis of catalysis, processes, and scope. Ind Eng Chem Res 2021;60(1):89–113.
[22] Basile A, Parmaliana A, Tosti S, Iulianelli A, Gallucci F, Espro C, Spooren J. Hydrogen production by methanol steam reforming carried out in membrane reactor on Cu/Zn/Mg-based catalyst. Catal Today 2008;137(1):17–22.
[23] Burnete NV, Mariasiu F, Depcik C, Barabas I, Moldovanu D. Review of thermoelectric generation for internal combustion engine waste heat recovery. Prog Energy Combust Sci 2022;91:101009.
[24] Tang Y, Wang Y, Long W, Xiao G, Wang Y, Li W. Analysis and enhancement of methanol reformer performance for online reforming based on waste heat recovery of methanol-diesel dual direct injection engine. Energy 2023;283:129098.
[25] Varshil P, Deshmukh D. A comprehensive review of waste heat recovery from a diesel engine using organic rankine cycle. Energy Rep 2021;7:3951–70.
[26] Bayramoğlu K. Determination of hydrogen production performance with waste exhaust gas in marine diesel engines. Int J Hydrogen Energy 2024;52:1319–33.
[27] Zhao N, Wang J, Yang J, Yuan F. Comprehensive evaluation and optimization strategy of solar-driven methanol steam reforming for hydrogen production. Renew Energy 2024;232:121120.

[28] Chen G, Shen Q, Zhang X, Zhao T, Zhu K, Li S. High purity H2 resource from methanol steam reforming at low-temperature by spinel CuGa2O4 catalyst for fuel cell. Ceram Int 2024.
[29] Huang M, Qifei BO, Juan LI, Jingxuan Qıa O, Shanliang Yuan, Zhang B, Jıang Y. Hydrogen production via steam reforming of methanol on Cu/ZnO/Al2O3 catalysts: effects of Al2O3 precursors. J Fuel Chem Technol 2024;52(10):1443–53.
[30] Achomo MA, Muthukumar P, Peela NR. Hydrogen production via steam reforming of methanol using Cu/ZnO/Al2O3: effect of catalyst synthesis method and Cu to Zn molar ratio on physico-chemical properties and catalytic performance. Int J Hydrogen Energy 2024.
[31] Alfuhaid LT, Nasser GA, Alabdulhadi RA, Khan MY, Yamani ZH, Helal A. Steam reforming of dodecane using Ni-red mud catalyst: a sustainable approach for hydrogen production. Int J Hydrogen Energy 2024;86:177–84.
[32] Ağbulut Ü, Bakır H, Mo HJ, Vozka P. Maximizing the hydrogen content for methanol steam reforming processes by using the novel pareto-based multi-objective evolutionary algorithms. Int J Hydrogen Energy 2024;90:1467–76.
[33] Bakır H, Kahraman HT, Yılmaz S, Duman S, Guvenc U. Dynamic switched crowding-based multi-objective particle swarm optimization algorithm for solving multi-objective AC-DC optimal power flow problem. Appl Soft Comput 2024;166:112155.
[34] Khodadadi N, Abualigah L, Mirjalili S. Multi-objective stochastic paint optimizer (MOSPO). Neural Comput Appl 2022;34(20):18035–58.
[35] Mirjalili S, Saremi S, Mirjalili SM, Coelho LDS. Multi-objective grey wolf optimizer: a novel algorithm for multi-criterion optimization. Expert Syst Appl 2016;47:106–19.
[36] Mosińska M, Szynkowska-Jóźwik MI, Mierczyński P. Catalysts for hydrogen generation via oxy–steam reforming of methanol process. Materials 2020;13(24):5601.
[37] Yadav NK, Saxena MR, Maurya RK. Environmental and cancer risk potential assessment of unregulated emissions from methanol-diesel dual fuel RCCI engine (No. 2024-26-0152). SAE Techn Paper 2024.
[38] Parris D, Spinthiropoulos K, Ragazou K, Giovou A, Tsanaktsidis C. Methanol, a plugin marine fuel for green house gas reduction—a review. Energies 2024;17(3):605.
[39] Kahraman HT, Akbel M, Duman S, Kati M, Sayan HH. Unified space approach-based Dynamic Switched Crowding (DSC): a new method for designing Pareto-based multi/many-objective algorithms. Swarm Evol Comput 2022;75:101196.
[40] Kennedy J, Eberhart R. Particle swarm optimization. Proceedings of 'ICNN'95-international conference on neural networks. vol. 4. ieee; 1995, November. p. 1942–8.
[41] Kaveh A, Talatahari S, Khodadadi N. Stochastic paint optimizer: theory and application in civil engineering. Eng Comput 2022:1–32.
[42] Mirjalili S, Mirjalili SM, Lewis A. Grey wolf optimizer. Adv Eng Software 2014;69:46–61.
[43] Myers RH, Montgomery DC, Anderson-Cook CM. Response surface methodology: process and product optimization using designed experiments. John Wiley & Sons; 2016.
[44] Zhao N, Wang J, Yao Z, Shao Y, Tian Y, Liu W. A novel multi-objective optimization model of solar-driven methanol steam reforming system combining response surface methodology and three-dimensional numerical simulation. Energy Convers Manag 2024;300:117986.
[45] Tang Y, Long W, Wang Y, Xiao G, Wang Y, Lu M. Multi-objective optimization of methanol reforming reactor performance based on response surface methodology and multi-objective particle swarm optimization coupling algorithm for on-line hydrogen production. Energy Convers Manag 2024;307:118377.
[46] Ghadikolaei MA, Yung K-F, Cheung CS, Lau P-C. Chemical properties and composition of PM emitted from a diesel engine fueled with ternary fuel (diesel-biodiesel-ethanol) in blended and fumigation modes. Fuel 2019;251:368–82.
[47] Kanth S, Debbarma S. Comparative performance analysis of diesel engine fuelled with hydrogen enriched edible and non-edible biodiesel. Int J Hydrogen Energy 2021;46(17):10478–93.
[48] Garcia G, Arriola E, Chen WH, De Luna MD. A comprehensive review of hydrogen production from methanol thermochemical conversion for sustainability. Energy 2021;217:119384.
[49] Dalena F, Senatore A, Marino A, Gordano A, Basile M, Basile A. Methanol production and applications: an overview. Methanol 2018:3–28.